Journal of Mathematical Research with Applications
Jan., 2025, Vol. 45, No. 1, pp. 73–83
DOI:10.3770/j.issn:2095-2651.2025.01.007
Http://jmre.dlut.edu.cn

A Decoupling-Type Strategy for the Allen-Cahn Equation on Curved Surfaces

Xiaoman XIE*, Qing PAN
School of Computer and Communication Engineering, Changsha University of Science & Technology, Hunan 410114*, P. R. China*

Abstract In this paper, we construct an efficient decoupling-type strategy for solving the Allen-Cahn equation on curved surfaces. It is based on an FEM-EIEQ (Finite Element Method and explicit-Invariant Energy Quadratization) fully discrete scheme with unconditional energy stability. Spatially the FEM is adopted, using a triangular mesh discretization strategy that can be adapted to complex regions. Temporally, the EIEQ approach is considered, which not only linearizes the nonlinear potential but also gives a new variable that we combine with the nonlocal splitting method to achieve the fully decoupled computation. The strategy can successfully transform the Allen-Cahn system into some completely independent algebraic equations and linear elliptic equations with constant coefficients, we only need to solve these simple equations at each time step. Moreover, we conducted some numerical experiments to demonstrate the effectiveness of the strategy.

Keywords FEM-EIEQ; Allen-Cahn equation; surface

MR(2020) Subject Classification 35B35; 35B40; 65J15

1. Introduction

Let $\Omega := \{x(\phi^1, \phi^2) \in \mathrm{R}^3 : (\phi^1, \phi^2) \in \mathcal{D} \subset \mathrm{R}^2\}$ be a sufficiently smooth and orientable surface. Note that the surface Ω considered in this study is a closed region, which does not have any boundary. Denote

$$C_k(\Omega) = \Big\{ f \in C^\infty(\Omega) : \int_\Omega |\nabla^i f|^2 \mathrm{d}x \le \infty, \quad i = 0, \dots, k \Big\}, \tag{1.1}$$

where k is a constant, f is a function, and the initial condition is $\nabla^0 f = f$. It is clear that $C_k(\Omega) = C^\infty(\Omega) \subset C^k(\Omega) \subset H^k(\Omega)$, here $H^k(\Omega)$ is the Sobolev space.

We consider a scalar function $u(x,t)$ that is governed by the Allen-Cahn equation as follows:

$$u_t = \epsilon^2 \Delta u - f(u), (x,t) \in \Omega \times (0,T], \tag{1.2}$$

where ϵ is the interface width, note that $\epsilon \ll 1$, $u|_{t=0} = u_0$, and $f(u)$ is a first-order derivative of the quartic density function

$$F(u) = \frac{1}{4}(u^2 - 1)^2. \tag{1.3}$$

Received January 4, 2024; Accepted March 8, 2024
Supported by the National Natural Science Foundation of China (Grant No. 12171147).
* Corresponding author
E-mail address: 22208051721@stu.csust.edu.cn (Xiaoman XIE); panqing@lsec.cc.ac.cn (Qing PAN)

The Allen-Cahn equation satisfies the diffusion rate of the total free energy

$$\frac{\mathrm{d}}{\mathrm{d}t}E(u) \leq 0, \tag{1.4}$$

where $E(u)$ is the Liapunov energy functional

$$E(u) = \int_{\Omega} (\frac{\epsilon^2}{2}|\nabla u|^2 + F(u))\mathrm{d}x. \tag{1.5}$$

The Allen-Cahn equation [1], a main phase-field model, is used to describe the phenomena of grain boundary evolution, phase separation, and phase transition in materials (e.g., growth of crystals). Nowadays, it has been widely used in many fields, such as condensed matter physics, computational biology, and image processing. It is always known that there is a stiffness issue in the Allen-Cahn equation, so the time step will be subject to strict stability limitations in the solution. Numerous relevant numerical strategies [2–8] have been developed in recent years to tackle it, but they all have some drawbacks, such as efficiency, computational cost, and stability problems. This paper aims to develop an efficient decoupled-type algorithm to solve the Allen-Cahn model on curved surfaces. We need to choose two suitable methods for the discretization in space and time respectively, then design a fully discrete algorithm that has high temporal accuracy.

In this paper, the FEM (Fine Element Method) [9] is used for the spatial discretization of surfaces, which is based on the variational principle and has some characteristics of the differential method. Compared with the finite difference method [10] and spectral method [11], which are only applicable to simple domains, the FEM is not only applicable to various complex regions but also has high computational accuracy, which can handle a variety of irregular surfaces in engineering applications with effectiveness. For the time discretization, we refer to the IEQ (Invariant Energy Quadratization) approach [12–23], an effective method for handling stiffness nonlinear terms in systems. However, it necessitates the time-consuming solution of linear systems with variable coefficients. For this reason, this study introduces a nonlocal variable on the IEQ method and designs an ODE (Ordinary Differential Equation) for it to make linear systems have only the constant-coefficient, i.e., the EIEQ (Explicit-Invariant Energy Quadratization) approach [24].

By combining these two methods, we offer a fully discrete FEM-EIEQ scheme for solving the Allen-Cahn equation and the proof of unconditional energy stability. Subsequently, we consider a non-local splitting technique to construct the fully decoupled strategy on this basis, then get some simple algebraic equations and linear elliptic equations that need to be solved at each time step, none of which have variable coefficients among them, greatly reducing the computational cost.

This paper's content is arranged as follows. In Section 2, we develop a fully discrete scheme based on FEM and EIEQ approach. A decoupling realization strategy for the fully discrete scheme is shown in Section 3. In addition, in Section 4, we put the established strategy into practice, and simulate some conclusions. Some conclusions are provided in Section 5.

2. The FEM-EIEQ scheme

This section introduces the FEM and the EIEQ approach, then designs a fully discretized scheme to solve Eq. (1.2).

2.1. Spatial discretization method

The FEM can be used for complex surfaces and non-uniform meshes. It dissects the surface and uses linear interpolation refinement to discretize the partial differential equations on the surfaces.

We triangulate the surface Ω into non-overlapping sub-triangles, then number these patches as $e_k, k = 1, \ldots, N_e$ and label their node sits as $P_i(w_i, v_i), i = 1, \ldots, N_p$. Let $H^2(\Omega_h)$ be the trial function space, where h denotes the maximum side length of the triangular region, and the process of decreasing h is the process of continual refinement of the dissection.

Take a patch e, with vertices P_i, P_j, P_m, and there exists $u_h = u_h(w, v) = aw+bv+c, (w, v) \in e$, where a, b, c are constants. By combining the functional equation $u_h(w, v)$ at the three vertices, we can obtain expressions for a, b and c, which all contain u_i, u_j and u_m. Substituting them into $u_h(w, v)$ yields:

$$u_h(w, v) = N_i(w, v)u_i + N_j(w, v)u_j + N_m(w, v)u_m, \tag{2.1}$$

where the basis functions satisfy

$$N_k(w_l, v_l) = \begin{cases} 0, & k \neq l, \\ 1, & k = l, \end{cases} \quad k, l = i, j, m. \tag{2.2}$$

It follows that the linear combination of basis functions $\phi_i(w, v)$, $i = 1, \ldots, N_p$ can be used to express any function in $H^2(\Omega_h)$:

$$u_h(w, v) = \sum_{i=1}^{N_p} u_i\phi_i(w, v), (w, v) \in \Omega, \tag{2.3}$$

where the value of the basis function $\phi_i(w, v)$ is 1 at P_i, and is nonzero only near node P_i.

Next, we briefly introduce two important concepts.

The elements of the total stiffness matrix $\boldsymbol{K}$ represent the interactions of the nodes. For node P_i, its element on $\boldsymbol{K}$ is k_{ii}. The value of k_{ii} is obtained by summing up k_{ii}^e in each element stiffness matrix $\boldsymbol{K}_{e_n}$. Since the value of $\phi_i(w, v)$ is non-zero only in the near vicinity of P_i, the non-zero element in row i of $\boldsymbol{K}$ exists only in the columns corresponding to the nodes neighboring P_i. It can be inferred that $\boldsymbol{K}$ is a sparse matrix when there are many nodes.

The total load vector $\boldsymbol{F}$ is the superposition of the cell load vectors $\boldsymbol{F}_{e_n}$ on each cell by rearranging the three components of the cell load vector according to the total number of nodes and expanding them into N_e-dimensional vectors (with the other elements being 0).

In the FEM, there may be more than one unit of external force and displacement, which correspond to different nodes and are coupled according to a certain relationship:

$$\boldsymbol{K}u - \boldsymbol{F} = 0. \tag{2.4}$$

2.2. Time-advance strategy

The EIEQ approach is designed with two auxiliary variables that are used to implement the "quadratization" of the nonlinear function and realize computational decoupling, respectively. There are some advantages of using this approach, which can transform the Allen-Cahn equation into an equivalent linear system with respect to the evolution of time, deal with the variable coefficients in it, and also accomplish the decoupling by splitting each equation into some independent sub-equations.

First, we design a nonlocal variable $G(u)$ for the quadratization of the function $F(u)$ which is bounded from below, shown as

$$G(u) = \sqrt{F(u) - \frac{s}{2}u^2 + B}, \tag{2.5}$$

where S and B are two fixed constants greater than zero. Since the energy potential $F(u)$ is a fourth-order polynomial, the S term is always constrained from below. Furthermore, to make sure that the radians are further positive, the constant B is introduced. We denote

$$H = 2\frac{\mathrm{d}}{\mathrm{d}u}G(u) = \frac{f(u) - Su}{\sqrt{F(u) - \frac{S}{2}u^2 + B}}. \tag{2.6}$$

Secondly, we define a nonlocal auxiliary variable $R(t)$, and design an ODE for it:

$$\begin{cases} R_t = (HG, u_t) - (Hu_t, G), \\ R|_{t=0} = 1. \end{cases} \tag{2.7}$$

Since $R_t = 0$ and $R|_{(t=0)} = 1$, it follows that $R(t) = 1$.

Now, we combine the original system (1.2) with Eqs. (2.5) and (2.7) to obtain the equivalent system that follows:

$$u_t = \epsilon^2 \Delta u - Su - RHG, \tag{2.8}$$

$$G_t = \frac{1}{2}RHu_t, \tag{2.9}$$

$$R_t = (HG, u_t) - (Hu_t, G). \tag{2.10}$$

The new transformation systems (2.8)–(2.10) have the following initial conditions:

$$\begin{cases} u|_{t=0} = u_0, \\ G|_{t=0} = \sqrt{F(u_0) - \frac{s}{2}u_0^2 + B}, \end{cases} \tag{2.11}$$

and the total free energy is updated to

$$E(u, R, G) = \int_\Omega (\frac{\epsilon^2}{2}|\nabla u|^2 + \frac{s}{2}|u|^2 + |G|^2 - B)\mathrm{d}x + \frac{1}{2}|R|^2 - \frac{1}{2}, \tag{2.12}$$

by integrating Eq. (2.9) over time, it can be derived that systems (2.8)–(2.10) and system (1.2) are equivalent. Moreover, the transformed systems (2.8)–(2.10) retain the energy dissipation law in Theorem 2.1.

Theorem 2.1 *The energy dissipation law of the systems (2.8)–(2.10) reads as follows:*

$$\frac{\mathrm{d}}{\mathrm{d}t}E(u,R,G)=-\|u_t\|^2\leq 0. \tag{2.13}$$

Proof We can take the L^2-inner product of Eq. (2.8) and u_t and conduct the integration by parts, then do the same for Eq. (2.9) and $2G$, Eq. (2.10) and R, respectively. The results are shown below:

$$(u_t,u_t)=-\epsilon^2(\nabla u,\nabla u_t)-S(u,u_t)-R(HG,u_t), \tag{2.14}$$

$$\frac{\mathrm{d}}{\mathrm{d}t}\int_\Omega |G|^2\mathrm{d}x=R(Hu_t,G), \tag{2.15}$$

$$\frac{\mathrm{d}}{\mathrm{d}t}(\frac{1}{2}|R|^2)=R(HG,u_t)-R(Hu_t,G). \tag{2.16}$$

Combining Eqs. (2.14)–(2.16), we can get Eq. (2.13). □

2.3. Fully discrete scheme

In order to fully discretize the new systems (2.8)–(2.10), we construct a numerical scheme in this section based on a second-order backward differential formulation and prove its unconditional energy stability. The time step is indicated by $\delta t>0$ and $t^n=n\delta t, 0\leq n\leq N$ with $T=N\delta t$.

Assume that u_h^n, G_h^n, R^n and $u_h^{n-1}, G_h^{n-1}, R^{n-1}$ are known, u_h^{n+1}, G_h^{n+1} and R^{n+1} are computed by the following numerical scheme:

$$(\frac{3u_h^{n+1}-4u_h^n+u_h^{n-1}}{2\delta t},\theta_h)=-\epsilon^2(\nabla u_h^{n+1},\nabla\theta_h)-S(u_h^{n+1},\theta_h)-R^{n+1}(H_h^*G_h^*,\theta_h), \tag{2.17}$$

$$(\frac{3G_h^{n+1}-4G_h^n+G_h^{n-1}}{2\delta t},\xi_h)=\frac{1}{2}R^{n+1}(H_h^*u_{ht}^*,\xi_h), \tag{2.18}$$

$$\frac{3R^{n+1}-4R^n+R^{n-1}}{2\delta t}=(H_h^*G_h^*,\frac{3u_h^{n+1}-4u_h^n+u_h^{n-1}}{2\delta t})-(H_h^*u_{ht}^*,G_h^{n+1}), \tag{2.19}$$

where $\theta_h,\xi_h\in H^2(\Omega_h)$ are test functions and

$$\begin{cases} u_h^*=2u_h^n-u_h^{n-1}, & G_h^*=2G_h^n-G_h^{n-1},\\ H_h^*=H(u_h^*), & u_{ht}^*=\frac{5u_h^n-8u_h^{n-1}+3u_h^{n-2}}{2\delta t}. \end{cases} \tag{2.20}$$

The schemes (2.17)–(2.19) appear to be fully coupled and unconditional energy stability.

Theorem 2.2 *The discrete energy dissipation law for schemes (2.17)–(2.19) is as follows:*

$$E^{n+1}-E^n\leq -\delta t\|\frac{3u_h^{n+1}-4u_h^n+u_h^{n-1}}{2\delta t}\|^2, \tag{2.21}$$

where E^k $(k>0)$ is the discrete energy:

$$\begin{aligned} E^k=&\frac{\epsilon^2}{4}(\|\nabla u_h^k\|^2+\|2\nabla u_h^k-\nabla u_h^{k-1}\|^2)+\frac{s}{4}(\|u_h^k\|^2+\|2u_h^k-u_h^{k-1}\|^2)+\\ &\frac{1}{2}(\|G_h^k\|^2+\|2G_h^k-G_h^{k-1}\|^2)+\frac{1}{4}(|R^k|^2+|2R^k-R^{k-1}|^2)-B|\Omega|-\frac{1}{2}. \end{aligned} \tag{2.22}$$

Proof First, there is a formula

$$2(3x-4y+z,x)=x^2-y^2+(2x-y)^2-(2y-z)^2+(x-2y+z)^2. \tag{2.23}$$

For Eq. (2.17), we take $\theta_h=\frac{3u_h^{n+1}-4u_h^n+u_h^{n-1}}{2\delta t}$, perform the integration by parts, and use Eq. (2.23) to have:

$$\begin{aligned}\delta t\|\frac{3u_h^{n+1}-4u_h^n+u_h^{n-1}}{2\delta t}\|^2=&-\frac{\epsilon^2}{4}(\|\nabla u_h^{n+1}\|^2-\|\nabla u_h^n\|^2+\|2\nabla u_h^{n+1}-\nabla u_h^n\|^2-\\&\|2\nabla u_h^n-\nabla u_h^{n-1}\|^2+\|\nabla u_h^{n+1}-2\nabla u_h^n+\nabla u_h^{n-1}\|^2)-\\&\frac{s}{4}(\|u_h^{n+1}\|^2-\|u_h^n\|^2+\|2u_h^{n+1}-u_h^n\|^2-\\&\|2u_h^n-u_h^{n-1}\|^2+\|u_h^{n+1}-2u_h^n+u_h^{n-1}\|^2)-\\&R^{n+1}(H_h^*G_h^*,\frac{3u_h^{n+1}-4u_h^n+u_h^{n-1}}{2}).\end{aligned} \tag{2.24}$$

For Eq. (2.18), we take $\xi_h=2\delta tG_h^{n+1}$ and use Eq. (2.23) to have:

$$\begin{aligned}&\frac{1}{2}(\|G_h^{n+1}\|^2-\|G_h^n\|^2+\|2G_h^{n+1}-G_h^n\|^2-\|2G_h^n-G_h^{n-1}\|^2+\\&\|G_h^{n+1}-2G_h^n+G_h^{n-1}\|^2)=\delta tR^{n+1}(H_h^*u_{ht}^*,G_h^{n+1}).\end{aligned} \tag{2.25}$$

Then we multiply Eq. (2.19) by δtR^{n+1}, and use Eq. (2.23) to have:

$$\begin{aligned}&\frac{1}{4}(|R^{n+1}|^2-|R^n|^2+|2R^{n+1}-R^n|^2-|2R^n-R^{n-1}|^2+|R^{n+1}-2R^n+R^{n-1}|^2)\\&=R^{n+1}(H_h^*G_h^*,\frac{3u_h^{n+1}-4u_h^n+u_h^{n-1}}{2})-\delta tR^{n+1}(H_h^*u_{ht}^*,G_h^{n+1}).\end{aligned} \tag{2.26}$$

Combining Eqs. (2.24)–(2.26) we can obtain

$$\begin{aligned}&\frac{\epsilon^2}{4}(\|\nabla u_h^{n+1}\|^2-\|\nabla u_h^n\|^2+\|2\nabla u_h^{n+1}-\nabla u_h^n\|^2-\|2\nabla u_h^n-\nabla u_h^{n-1}\|^2+\\&\|\nabla u_h^{n+1}-2\nabla u_h^n+\nabla u_h^{n-1}\|^2)+\\&\frac{s}{4}(\|u_h^{n+1}\|^2-\|u_h^n\|^2+\|2u_h^{n+1}-u_h^n\|^2-\|2u_h^n-u_h^{n-1}\|^2+\|u_h^{n+1}-2u_h^n+u_h^{n-1}\|^2)+\\&\frac{1}{2}(\|G_h^{n+1}\|^2-\|G_h^n\|^2+\|2G_h^{n+1}-G_h^n\|^2-\|2G_h^n-G_h^{n-1}\|^2+\|G_h^{n+1}-2G_h^n+G_h^{n-1}\|^2)+\\&\frac{1}{4}(|R^{n+1}|^2-|R^n|^2+|2R^{n+1}-R^n|^2-|2R^n-R^{n-1}|^2+|R^{n+1}-2R^n+R^{n-1}|^2)\\=&-\delta t\|\frac{3u_h^{n+1}-4u_h^n+u_h^{n-1}}{2\delta t}\|^2,\end{aligned} \tag{2.27}$$

which implies that the schemes (2.17)–(2.19) are unconditionally energy stable. □

3. The decoupled strategy

This section uses a non-local splitting technique to realize the fully decoupled computing of the schemes (2.17)–(2.19). Split u_h^{n+1} and G_h^{n+1} as:

$$u_h^{n+1}=u_{1h}^{n+1}+R^{n+1}u_{2h}^{n+1},G_h^{n+1}=G_{1h}^{n+1}+R^{n+1}G_{2h}^{n+1}, \tag{3.1}$$

then we solve $u_{1h}^{n+1},u_{2h}^{n+1}$ and $G_{1h}^{n+1},G_{2h}^{n+1}$.

After substituting u_h^{n+1} in the systems (2.17) and (2.18) using Eq. (3.1), we break down the resulting equations based on R^{n+1} into systems:

$$(\frac{3u_{1h}^{n+1}-4u_h^n+u_h^{n-1}}{2\delta t},\theta_h)=-\epsilon^2(\nabla u_{1h}^{n+1},\nabla\theta_h)-S(u_{1h}^{n+1},\theta_h), \tag{3.2}$$

$$(\frac{3u_{2h}^{n+1}}{2\delta t},\theta_h)=-\epsilon^2(\nabla u_{2h}^{n+1},\nabla\theta_h)-S(u_{2h}^{n+1},\theta_h)-(H_h^*G_h^*,\theta_h), \tag{3.3}$$

$$(\frac{3G_{1h}^{n+1}}{2\delta t},\xi_h)=(\frac{4G_h^n-G_h^{n-1}}{2\delta t},\xi_h), \tag{3.4}$$

$$(\frac{3G_{2h}^{n+1}}{2\delta t},\xi_h)=\frac{1}{2}(H_h^*u_{ht}^*,\xi_h). \tag{3.5}$$

As can be seen, these systems are easy to solve. Eqs. (3.2) and (3.3) are linear elliptic, including just constant-coefficients, while Eqs. (3.4) and (3.5) are algebraic.

Use the solutions u_h^{n+1} and G_h^{n+1} of Eqs. (3.2)–(3.5) to update R^{n+1} in Eq. (2.19):

$$(\frac{3}{2\delta t}-\varphi_1)R^{n+1}=\frac{1}{2\delta t}(4R^n-R^{n-1})+\varphi_2, \tag{3.6}$$

where

$$\begin{cases}\varphi_1=(H_h^*G_h^*,\frac{3u_{2h}^{n+1}}{2\delta t})-(H_h^*u_{ht}^*,G_{2h}^{n+1}),\\ \varphi_2=(H_h^*G_h^*,\frac{3u_{1h}^{n+1}-4u_h^n+u_h^{n-1}}{2\delta t})-(H_h^*u_{ht}^*,G_{1h}^{n+1}).\end{cases} \tag{3.7}$$

The Eq. (3.6) is solvable and is proved as follows:

Setting $\theta_h=\frac{3}{2\delta t}u_{2h}^{n+1}$ in Eq. (3.3) gives

$$\|\frac{3u_{2h}^{n+1}}{2\delta t}\|^2+\frac{3\epsilon^2}{2\delta t}\|\nabla u_{2h}^{n+1}\|^2+\frac{3S}{2\delta t}\|u_{2h}^{n+1}\|^2=-(H_h^*G_h^*,\frac{3u_{2h}^{n+1}}{2\delta t}). \tag{3.8}$$

Set $\xi_h=2G_{2h}^{n+1}$ in Eq. (3.5) to get

$$\|\frac{3G_{2h}^{n+1}}{\delta t}\|^2=(H_h^*u_h^*,G_{2h}^{n+1}). \tag{3.9}$$

Combining Eqs. (3.8) and (3.9) gives $\varphi_1\le 0$, so $\frac{3}{2\delta t}-\varphi_1\neq 0$ and Eq. (3.6) is solvable.

Up to this point, all variables are decoupled using the previously described decoupling method, and the scheme has just constant coefficients, resulting in exceptionally efficient computations in practice.

4. Numerical experiments

The numerical examples performed in this section all use the GMS solver (set to a sufficiently long number of iterations) to solve the approximate solution.

In the first test, we do a numerical simulation to evaluate the suggested strategy's convergence rates. Here, the computational domain as $\Omega=\{(x,y,z):\sqrt{x^2+y^2+z^2}=1\}$, and parameters are set as $\epsilon=1\mathrm{e}-4, S=4, B=1\mathrm{e}4$. In addition, the initial condition as $u_0=0.1\cos(2x)+0.2\cos(y)$. We use the solution from the strategy calculation at the time step $t=2.56\mathrm{e}-1$ as

the benchmark solution (approximate exact solution) to compute the model's error because the exact solution is unknown. Figure 1 displays the scheme's L^2 numerical error, which indicates that the scheme possesses second-order spatial precision.

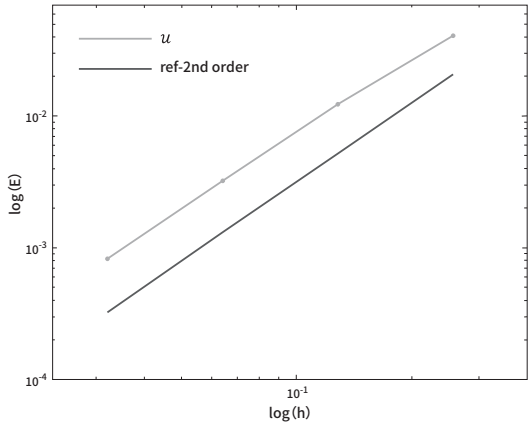

Figure 1 The L^2 numerical error of u

In some of the next experiments, we investigate the spinodal decomposition (phase separation) using the developed strategy. Define the computational domain as some closed and set

$$u_0 = 0.001\,\mathrm{rand}(x, y, z), \mathrm{rand}(x, y, z) \in [-1, 1]. \tag{4.1}$$

Note that the random numbers have a mean of zero.

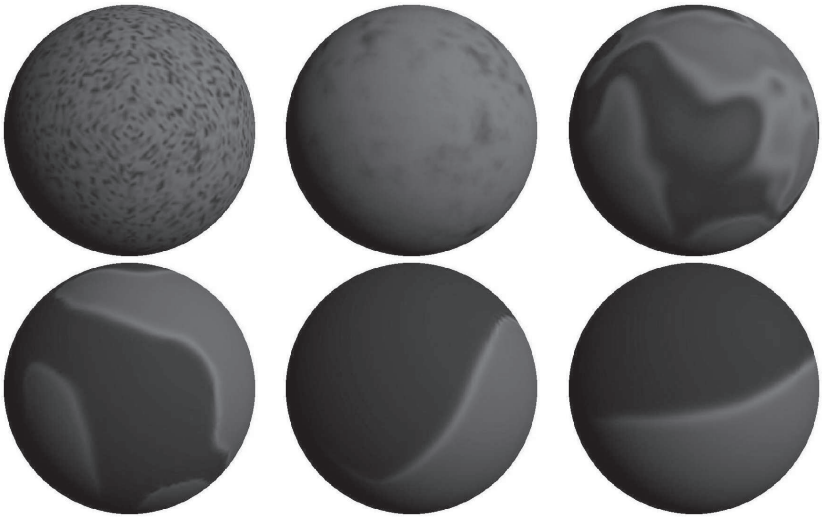

Figure 2 Snapshots of the phase variable u for Ω_1

Set the computational domain to the sphere $\Omega_1 = \{(x, y, z) : \sqrt{x^2 + y^2 + z^2} = 10\}$, let $\epsilon = 3\mathrm{e} - 2, S = 4, B = 7\mathrm{e}3$, the snapshots of the profile can be obtained as shown in Figure 2, which plots u at different times of 0, 5, 20, 40, 200 and 8000 with time step $\delta t = 3\mathrm{e} - 2$. Moreover, we also obtained Figures 3 and 4, the former with the computational domain as an

annular $\Omega_2 = \{(x, y, z) : x \in [-4.98, 4.98], y \in [-4.98, 4.98], z \in [-1.32, 1.32]\}$, and parameters are $\epsilon = 6\text{e} - 3, S = 4, B = 8\text{e}3$. The figure shows the phase variable u for $\delta t = 1\text{e} - 2$ where snapshots are taken at $t = 0, 5, 20, 200, 280$ and 6000, respectively. The latter is a bunny surface $\Omega_3 = \{(x, y, z) : x \in [-9.12, 6.27], y \in [-3.38, 18.72], z \in [-6.49, 6.08]\}$ with parameters are $\epsilon = 5\text{e} - 3$, $S = 4$, $B = 9\text{e}3$, the displayed snapshots were taken by u at $t = 0, 20, 40, 100, 400$ and 6000 with $\delta t = 4\text{e} - 3$.

Figure 3 Snapshots of the phase variable u for Ω_2

Figure 4 Snapshots of the phase variable u for Ω_3

Over time, the system can evolve from a uniform state to a two-phase state. We can observe that the light gray region ($u = 1$) slightly shrinks while the dark region ($u = -1$) expands because of the non-conserved nature of the Allen-Cahn equation.

Finally, we tested the evolution of the free energy generalizations for some different time-step sizes for the numerical example given in Figure 3 and found that the energy profile decreases monotonically for all time steps, which demonstrates the unconditional energy stability of the strategy. In Figure 5, we give the evolution of free energy generalized functions for the numerical example in Figure 3 at $\delta t = 1\mathrm{e}-2, \delta t = 5\mathrm{e}-3, \delta t = 2.5\mathrm{e}-3$.

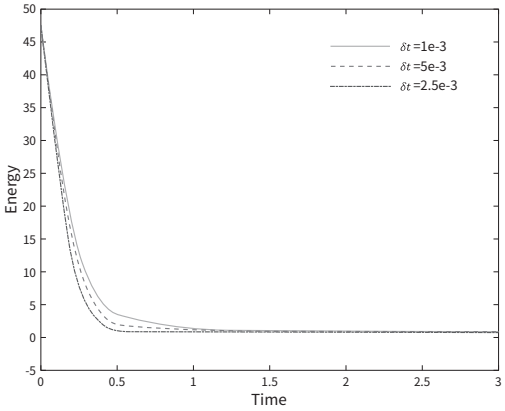

Figure 5 Evolutions of the free energy

5. Concluding remarks

In this paper, we develop a fully discrete numerical scheme combining FEM and EIEQ, then further propose a decoupling-type implementation strategy for solving the Allen-Cahn equation. The linear, unconditionally energy-stabilized, fully decoupled numerical strategy is obtained by combining the FEM with the EIEQ method and then processing it using a nonlocal splitting technique, which applies to a wide range of complex regions and can be used for problems with highly rigid nonlinear terms. Compared to other schemes, the strategy we provide significantly reduces the computational cost as it only requires solving a few fully decoupled simple equations (linear elliptic equations with only constant coefficients and algebraic equations) at each time step. Finally, by simulating some numerical examples, we demonstrate the developed scheme's efficacy.

Acknowledgements We thank the referees for their time and comments.

Conflict of Interest The authors declare no conflict of interest.

References

[1] S. M. ALLEN, J. W. CAHN. *A microscopic theory for antiphase boundary motion and its application to antiphase domain coarsening*. Acta Metall. Mater., 1979, **27**(6): 1085–1095.

[2] C. L. D. VAZ, J. L. BOLDRINI. *A mathematical analysis of a nonisothermal Allen-Cahn type system: error estimates*. Math. Methods Appl. Sci., 2012, **35**(12): 1406–1414.

[3] H. G. LEE, J. KIM. *An efficient and accurate numerical algorithm for the vector-valued Allen-Cahn equations*. Comput. Phys. Commun., 2012, **183**(10): 2107–2115.

[4] K. YASIR, A. ISHTIAQ, Qingbiao WU, et al. *Some new computational methods for the Allen-Cahn equation with non-periodic boundary conditions arising in computational fluid dynamics*. Int. J. Numer. Method. H., 2012, **23**(4): 588–597.

[5] Linlin BU, Liquan MEI, Yan HOU. *Stable second-order schemes for the space-fractional Cahn-Hilliard and Allen-Cahn equations*. Comput. Math. Appl., 2019, **78**(11): 3485–3500.

[6] S. HUSSAIN, A. SHAH, S. AYUB, et al. *An approximate analytical solution of the Allen-Cahn equation using homotopy perturbation method and homotopy analysis method*. Heliyon., 2019, **5**(12): e03060.

[7] Huan LIU, Aijie CHENG, Hong WANG. *A fast Galerkin finite element method for a space-time fractional Allen-Cahn equation*. J. Comput. Appl. Math., 2020, **368**: 112482, 18 pp.

[8] Hong ZHANG, Jingye YAN, Xu QIAN, et al. *Numerical analysis and applications of explicit high order maximum principle preserving integrating factor Runge-Kutta schemes for Allen-Cahn equation*. Appl. Numer. Math., 2021, **161**: 372–390.

[9] J. W. BARRETT, J. F. BLOWEY. *Finite element approximation of a degenerate Allen-Cahn/Cahn-Hilliard system*. SIAM J. Numer. Anal., 2002, **39**(5): 1598–1624.

[10] G. E. FORSYTHE, W. R. WASON. *Finite-Difference Methods for Partial Differential Equations*. John Wiley & Sons, Inc., New York-London, 1960.

[11] H. G. LEE, J. LEE. *A semi-analytical Fourier spectral method for the Allen-Cahn equation*. Comput. Math. Appl., 2014, **68**(3): 174–184.

[12] Jia ZHAO, Qi WANG, Xiaofeng YANG. *Numerical approximations for a phase field dendritic crystal growth model based on the invariant energy quadratization approach*. Int. J. Numer. Meth. Eng., 2017, **110**(3): 279–300.

[13] Xiaofeng YANG, Jia ZHAO, Qi WANG, et al. *Numerical approximations for a three-component Cahn-Hilliard phase-field model based on the invariant energy quadratization method*. Math. Models Methods Appl. Sci., 2017, **27**(11): 1993–2030.

[14] Xiaofeng YANG, Haijun YU. *Efficient second order unconditionally stable schemes for a phase field moving contact line model using an invariant energy quadratization approach*. SIAM J. Sci. Comput., 2018, **40**(3): B889–B914.

[15] Ruihan GUO, Yan XU. *Semi-implicit spectral deferred correction method based on the invariant energy quadratization approach for phase field problems*. Commun. Comput. Phys., 2019, **26**(1): 87–113.

[16] Zhengguang LIU, Xiaoli LI. *Efficient modified stabilized invariant energy quadratization approaches for phase-field crystal equation*. Numer. Algorithms, 2019, **85**(1): 1–26.

[17] Chaolong JIANG, Wenjun CAI, Yushun WANG. *A linearly implicit and local energy-preserving scheme for the sine-Gordon equation based on the invariant energy quadratization approach*. J. Sci. Comput., 2019, **80**(3): 1629–1655.

[18] Chuanjun CHEN, Kejia PAN, Xiaofeng YANG. *Numerical approximations of a hydro-dynamically coupled phase-field model for binary mixture of passive/active nematic liquid crystals and viscous fluids*. Appl. Numer. Math., 2020, **158**: 1–21.

[19] Jun ZHANG, Chuanjun CHEN, Xiaofeng YANG, et al. *Efficient numerical scheme for a penalized Allen-Cahn type Ohta-Kawasaki phase-field model for diblock copolymers*. J. Comput. Appl. Math., 2020, **378**: 112905, 23 pp.

[20] Xiaofeng YANG, Zhenlu CUI, M. G. FOREST, et al. *Dimensional robustness and instability of sheared, semidilute, nanorod dispersions*. Multiscale model. Sim., 2008, **7**(2): 622–654.

[21] Xiaofeng YANG. *Numerical approximations of the Navier-Stokes equation coupled with volume-conserved multi-phase-field vesicles system: fully-decoupled, linear, unconditionally energy stable and second-order time-accurate numerical scheme*. Comput. Methods Appl. Mech. Engrg., 2021, **375**: Paper No. 113600, 30 pp.

[22] Qi LI, Liquan MEI, Xiaofeng YANG, et al. *Efficient numerical schemes with unconditional energy stabilities for the modified phase field crystal equation*. Adv. Comput. Meth., 2019, **45**(3): 1551–1580.

[23] Jun ZHANG, Xiaofeng YANG. *Numerical approximations for a new L^2-gradient flow based phase field crystal model with precise nonlocal mass conservation*. Comput. Phys. Commun., 2019, **243**: 51–67.

[24] Xiaofeng YANG. *On a novel full decoupling, linear, second-order accurate, and unconditionally energy stable numerical scheme for the anisotropic phase-field dendritic crystal growth model*. Internat. J. Numer. Methods Engrg., 2021, **122**(16): 4129–4153.